Development of a Quantitative Intracranial Vascular Features Extraction Tool on 3D MRA Using Semiautomated Open-Curve Active Contour Vessel Tracing

Li Chen,[1] Mahmud Mossa-Basha,[2] Niranjan Balu,[2] Gador Canton,[2] Jie Sun,[2] Kristi Pimentel,[2] Thomas S. Hatsukami,[3] Jenq-Neng Hwang,[1] and Chun Yuan[2]*

Purpose: To develop a quantitative intracranial artery measurement technique to extract comprehensive artery features from time-of-flight MR angiography (MRA).

Methods: By semiautomatically tracing arteries based on an open-curve active contour model in a graphical user interface, 12 basic morphometric features and 16 basic intensity features for each artery were identified. Arteries were then classified as one of 24 types using prediction from a probability model. Based on the anatomical structures, features were integrated within 34 vascular groups for regional features of vascular trees. Eight 3D MRA acquisitions with intracranial atherosclerosis were assessed to validate this technique.

Results: Arterial tracings were validated by an experienced neuroradiologist who checked agreement at bifurcation and stenosis locations. This technique achieved 94% sensitivity and 85% positive predictive values (PPV) for bifurcations, and 85% sensitivity and PPV for stenosis. Up to 1,456 features, such as length, volume, and averaged signal intensity for each artery, as well as vascular group in each of the MRA images, could be extracted to comprehensively reflect characteristics, distribution, and connectivity of arteries. Length for the M1 segment of the middle cerebral artery extracted by this technique was compared with reviewer-measured results, and the intraclass correlation coefficient was 0.97.

Conclusion: A semiautomated quantitative method to trace, label, and measure intracranial arteries from 3D-MRA was developed and validated. This technique can be used to facilitate quantitative intracranial vascular research, such as studying cerebrovascular adaptation to aging and disease conditions. **Magn Reson Med 79:3229–3238, 2018. © 2017 International Society for Magnetic Resonance in Medicine.**

Key words: intracranial artery; vessel tracing; feature extraction; open-curve active contour; MR angiogram; time-of-flight

INTRODUCTION

Vascular structure and function are important factors for maintaining brain health. Increasing evidence indicates that cerebrovascular disease is an underrecognized contributor to dementia, even in the absence of brain infarctions (1,2). A more comprehensive description of the whole intracranial vascular map, as well as an accurate quantification of vascular features, could allow us to understand the effects of aging and other physiological/pathophysiological conditions on cerebral arteries and how such vascular changes impact brain health. Three-dimensional time-of-flight (TOF) MR angiography (MRA) (3) is widely used clinically to depict vascular anatomy and pathology (4–6). Current clinical review of MRA focuses on distinct stenoses or aneurysms in only the major arterial segments. Comprehensive feature extraction using automated algorithms may provide a detailed map of intracranial arteries from routine MRA, with global as well as regional information on blood supply that have been largely neglected.

However, it is challenging to comprehensively characterize cerebral arteries from MRA images because the cerebral vasculature is a complex network with substantial interindividual variation (7). In addition, small but anatomically important arteries such as communicating arteries are harder to detect due to their relatively weak signal resulting from slow or in-plane blood flow. An effective feature extraction method that can identify both large and small cerebral arteries, as well as provide quantitative cerebrovascular information on MRA, is critically needed for complete feature extraction.

To date, there has been little effort to measure features from vascular maps beyond 3D visualization, vessel segmentation, and identification of stenosis or absent arteries (8–10). Some existing vascular feature extraction tools (11,12) are limited to four morphometric features from each of the four anatomic regions of the intracranial arteries. Wright et al. (13) used L-Measure, an open-source tool to quantify 19 morphometric features from six major arteries stemming from the circle of Willis (CoW). However, tracing more distal arteries and labeling arteries in more precise categories could facilitate more detailed analysis.

In this study, we aimed to develop a comprehensive semiautomated intracranial artery feature-extraction technique using improved approaches for automated vessel tracing and labeling. Automated vessel tracing, which converts raw pixel or voxel content in planar or volumetric images to a topological and geometrical network with

[1]Department of Electrical Engineering, University of Washington, Seattle, Washington, USA.

[2]Department of Radiology, University of Washington, Seattle, Washington, USA.

[3]Department of Surgery, University of Washington, Seattle, Washington, USA.

Grant sponsor: National Institutes of Health; Grant numbers: R01-NS083503-03, R01-NS092207-01A1, R01-HL103609-01A1 and 1R56NS092207; Grant sponsor: Philips Healthcare.

*Correspondence to: Chun Yuan, PhD, Department of Radiology, University of Washington, Box 358050, 850 Republican St, Rm 127, Seattle, WA 98109-4714. E-mail: cyuan@uw.edu

Received 10 July 2017; revised 13 September 2017; accepted 18 September 2017

DOI 10.1002/mrm.26961

Published online 17 October 2017 in Wiley Online Library (wileyonlinelibrary.com).

centerline and radius, is the most important step for vascular feature extraction, as demonstrated from applications of retinal fundus images (14,15) and CT coronary angiography (16,17). Tracing by using the active contour model (snake) allows one to handle changes of topology and adapt locally to the shape of complex structures (18). The open-curve active contour model (19), which is one of its improvements and is driven by gradient vector flow (GVF) and traces without initial boundary, has been successfully applied in tracing neural fibers (19–21) as well as tree-like tubular structures (22), including cerebral vessels from CT angiography images (23). Recently, the application of a neuronal tree reconstruction method to MRA images has proved to be successful (13). With similar intention, the open-curve active contour model is likely to be suitable for MRA artery tracing after some modification and optimization, based on its adaptive stretching forces and smoothness preservation ability.

Moreover, the features provided by most existing 3D visualization and analysis tools (24,25) are limited to global geometric features such as length and volume, whereas regional features provide more direct information on vascular diseases (26,27). In addition, flow-dependent intensity features, which are often ignored in current segmentation algorithms, have potential value for the characterization of intracranial arteries. For example, high middle cerebral artery (MCA) velocity was found to be predictive of stroke in children with sickle cell disease (28).

Regional features are only available when all the arteries are correctly labeled. Therefore, we developed a new method for automated labeling to avoid labor intensive manual placement of branch points required by most current methods (11,12). Although other automatic labeling methods exist, they cannot be easily applied to comprehensive intracranial artery labeling (29,30) because those models cannot differentiate enough artery types (>24 types) to describe a complete arterial tree.

Therefore, the goal of this study was to develop a semiautomated intraCranial artery feature extraction (iCafe) technique that can comprehensively quantify morphometric and intensity features of intracranial arteries on MRA images. Based on an automated approach to artery tracing and labeling, interactive human supervision can be performed to ensure accuracy. Initial comparison with neuroradiologist review was performed to validate iCafe. By providing additional information on cerebrovascular structure and function beyond what is currently collected on MRA, iCafe presents a new opportunity to gain pathophysiological insights into the processes of vascular adaptation to aging and disease conditions in future population studies.

METHODS

MR Imaging

The algorithm was tested using eight prospectively recruited subjects (54 ± 17 years, 5 males), with clinically documented intracranial arterial stenosis likely to be secondary to atherosclerosis on clinical computed tomography angiography (CTA). Patients with clinically suspected central nervous system vasculitis, intracranial dissection, previous cranial trauma, previous radiation, and reversible cerebral vasoconstriction syndrome—or patients who underwent prior intracranial arterial interventions—were excluded from the study. Patients were scanned on a 3T Philips Ingenia Scanner (Philips Healthcare, Best, the Netherlands) using a standard head coil. Three-dimensional TOF MRA imaging parameters were as follows: Repetition time/echo time = 14.7/3.5 ms, flip angle = 18°, in-plane resolution = $0.3\,\text{mm} \times 0.3\,\text{mm}$, slice thickness = 1.4 mm, field of view = 190 mm*190 mm, matrix = 360*228, and acquisition time = 116.79 ± 21.57 s. Local institutional review board approval was obtained for all study procedures, and all subjects provided informed consent prior to enrollment.

Feature Extraction

The open-curve active contour model was originally designed as a neural fiber tracing method. However, the neural fiber tracing method is not ideal for vessel tracing given the different nature and scale of vessels compared to neurons. Therefore, a series of modifications to the open-curve active contour model were applied to trace vessels: 1) re-slicing, intensity normalization, and rudimentary segmentation before tracing; and 2) a combined tracing approach with both original image and vesselness image, described in further detail below. In addition, arteries were labeled for feature calculation after tracing.

The iCafe feature extraction process can be divided into image preprocessing, rudimentary segmentation, vessel tracing, artery labeling, feature calculation, and output. The workflow, along with example images at each stage, are shown in Figure 1.

Image Preprocessing

MRA images were resliced using bicubic interpolation to achieve isotropic resolution in 3D space; as in most cases, the voxels were anisotropic. The absolute intensity values of MR images do not have a fixed meaning; thus, a fast and accurate intensity normalization method by Nyul (31) was used to adjust intensities among cases in the database. Based on the assumption that the histogram of each MRA image is similar, intensities of interest (IoI) (10 percentiles as well as lower (0%) and higher (99.8%) percent intensity values) were trained to find parameters of standard scale. In the transformation stage, the IoI of each image was then mapped to the standard histogram by a lookup table (LUT). The original intensity of each voxel was then updated through the corresponding LUT.

Rudimentary Segmentation

A clear separation between background and vessel pixels will enhance the gradient vector and benefit the detection of small arteries. For this reason, rudimentary segmentation of the artery region using intensity thresholding was applied before tracing. The Phansalkar local threshold method (32) was used due to its local thresholding ability, with minimum loss of vascular regions in a reasonable processing time.

However, because the Phansalkar thresholding was not suitable for 3D visualization, the Renyi entropy

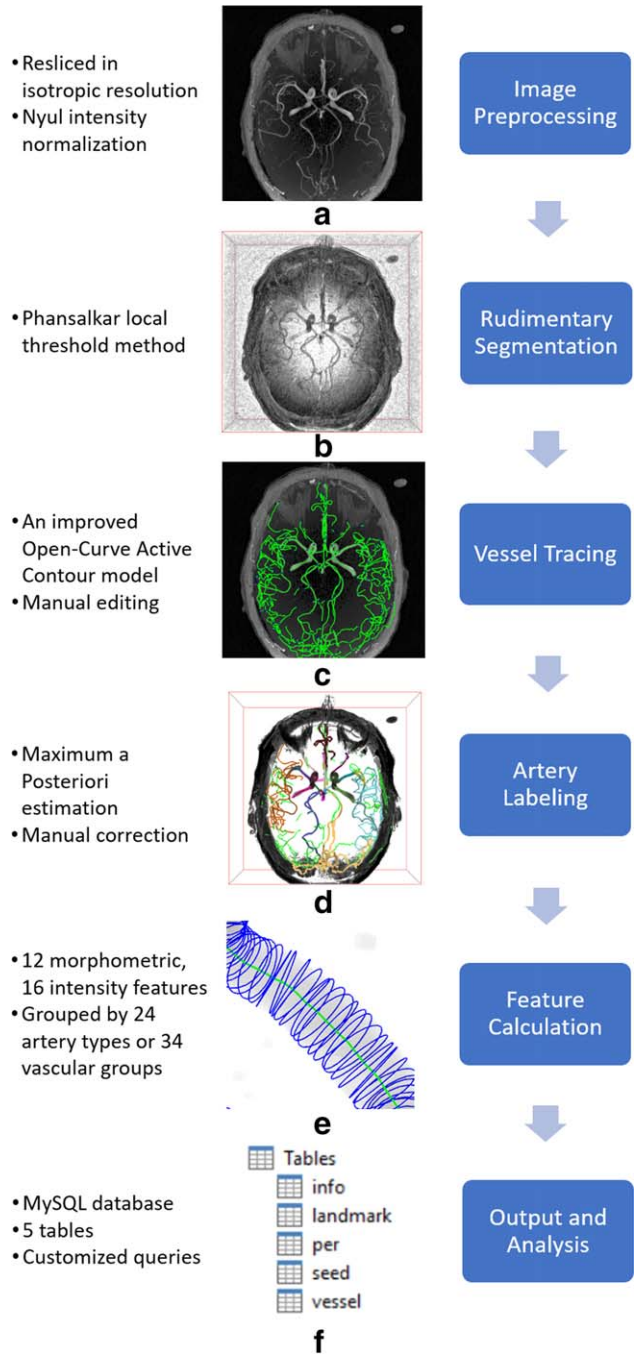

FIG. 1. Workflow for intraCranial artery feature extraction (the raw image is shown in (a) and (c), the Phansalkar thresholded image is shown in (b), and the Renyi thresholded image is shown in (d)).

threshold method (33), a method that can remove most background signal with the cost of some artery details, was also used. It should be noted that artery tracing was based on Phansalkar thresholded images to ensure capability of detecting small arteries, and traced results were reconstructed and superposed into Renyi thresholded images with clearer background for better visualization (Phansalkar thresholded image shown in Fig. 1b; Renyi thresholded image shown in Fig. 1d). With this approach, users can see an accurately traced arterial tree clearly.

Vessel Tracing

We improved the open-curve active contour model (19) for a high-quality vessel tracing for MRA. With the original open-curve active contour model, it is likely that two vessels in close proximity would be traced as one, which is particularly problematic for parallel arteries such as the anterior cerebral arteries (ACA). Because the active contour model (snake) traces through iterations (18), the trace initialized by a seed point is stretched toward the direction of largest tubular probability calculated from gradient vector in trace endpoints. (19). This gradient-based approach ensures elasticity and smoothness but is limited in its ability to differentiate parallel vessels because the intensity value between vessels is not low enough to form strong gradient vectors to confine traces to artery regions. Therefore, a combined tracing method using both raw and vesselness images (Frangi vesselness filtered (34) image) was devised to improve tracing of parallel vessels, which works as follows: Initially, the geometric center points of each connected region beyond a certain threshold in the vesselness image, called *seed points*, are found. In the first stage, the tracing process starts stretching from the seed point according to intensity value from the vesselness image. The current length of vessels is calculated in each iteration. If the length increases slower than 5% after an iteration, the trace is then stretched based on the raw image instead as a second stage until the length increase is below 5% after an iteration again or until a maximum iteration number is reached. The two-stage process also overcomes a well-known disadvantage of the Frangi filter that vessels near an arterial bifurcation are weakened after filtering (35) because the locally tubular structure does not apply to the area of branching. The first stage of tracing ensures the accuracy in parallel vessels, and the second stage avoids the vessel being cut off near bifurcation points.

Manual Editing

As a semiautomated technique, human supervision and correction are feasible when using iCafe to ensure the best quality of tracing. Three visualization methods (maximum intensity projection (MIP) view, 3D view, and cross-section view) are provided for observing artery details, as shown in Figure 2. Each trace in the MIP view or 3D view can be selected and edited. The operations available for users include the following: merging two traces together, splitting one trace into two, creating branch connections between traces, trimming endpoints of a trace, deleting traces, or removing outlier unconnected traces. Seed points can also be added manually, from which additional arteries can be traced using the same automatic tracing method.

Artery Labeling

Artery labeling and categorization are necessary after all vessels are traced to extract arterial segment-specific features. Therefore, a semiautomated labeling method was implemented. Twenty-four common artery types are assigned (definition of artery types in Supporting Table S1) based on 31 types of bifurcations of interest (BoI)

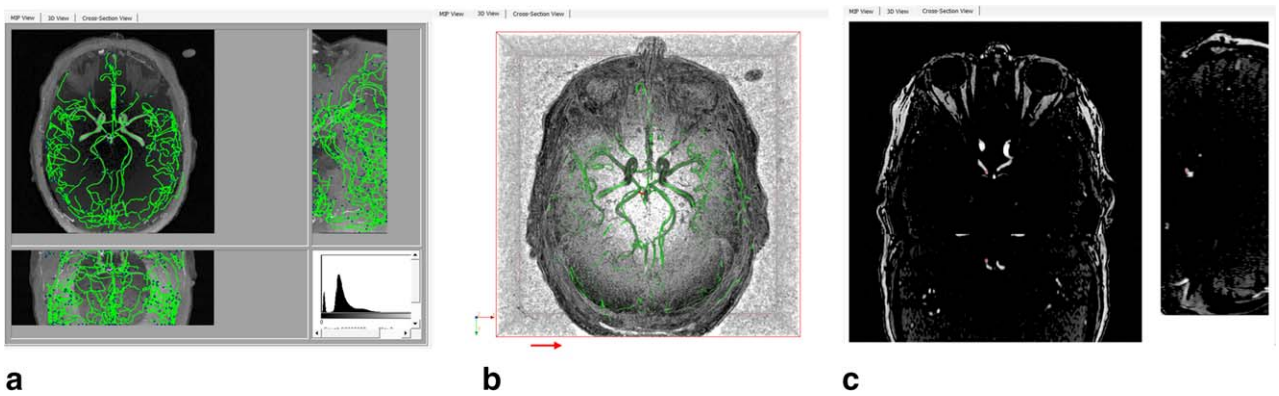

FIG. 2. Manual editing is facilitated by three views: (**a**) maximum intensity projection view with tracing results (green lines), (**b**) 3D view with tracing results (green lines), and (**c**) cross-section view.

that are identified automatically. For those traces with no label, BoI types are excluded because they are possibly distal vessels beyond the named branches.

The identification of BoI type is based on a probability model using the positional, directional, and topological features.

- Positional likelihood: Assumes BoI positions of each bifurcation type to follow Gaussian distribution, and calculates probability density function (pdf) of each bifurcation type from all the cases in the training set (previously processed data). Positional likelihood of the BoI for each bifurcation type was calculated from the corresponding pdf over the maximum probability in that function.
- Directional fitness: Averaged branch directions for each BoI type was calculated and normalized as model type based on previous labeled data. Each unlabeled BoI was then paired with an optimal model type by calculating and finding the maximum sum of inner product of all corresponding branch directions from each model type.
- Graph topological likelihood: a structural metric network structural index (NSI) (36) of BoI, which is a weighted addition based on graph topological connection that includes node degree, radius, and vesselness intensity, as well as their nearby neighbor nodes. Large vessels with more connections to neighbor nodes had larger NSI. Similar to positional likelihood, the model assumes the NSI of each bifurcation type to follow a Gaussian distribution and calculates topological likelihood from the pdf.

Using maximum a posteriori estimation, the possibilities of each bifurcation to be each BoI type were calculated. The labeling procedure was applied sequentially. Starting from the BoI with the highest probability and least ambiguity (largest difference between first and second possible types), BoI type was assigned in order. The prior probability of all neighbors was updated when a BoI type was assigned. Human inspection and correction were then performed to correct for errors.

Each artery could be labeled after all BoI types were assigned. Arteries with similar geometric and anatomical properties can be further grouped together based on anatomy and flow distribution. The 13 vascular groups are defined (definition of vascular group in Supporting Table S2). Some of the vascular groups also have subgroups to differentiate left- or right-side features.

Feature Calculation

Based on the labeled arteries, morphometric features and intensity features are calculated for each artery.

The 12 morphometric features are length, volume (assuming artery as a cylinder with changing radius), tortuosity (length over head–tail distance), surface area, average radius, minimum bifurcation angle, cross-section area, order (bifurcations toward internal carotid artery (ICA) for anterior arteries or vertebral artery (VA) for posterior arteries), distance to CoW, width (minimum sagittal span), depth (minimum coronal span), and height (minimum vertical span).

The 16 intensity features are max, min, mean, median, 10 percentiles (0%, 10%, ..., 90%), sigma, and sum. The intensity values are sampled from centerline points along arteries from intensity normalized images for calculation.

With 12 morphometric features and 16 intensity features for each artery, grouped by each of the 24 artery types or 34 vascular groups (6 overlaps), there could be a total of $(12+16)*(24+34-6)=1{,}456$ features extracted for each MRA.

Output and Analysis

Artery traces were saved in SWC format (37). Each line presents a point, which is comprised of sample number, BoI type, x position, y position, z position, radius, and parent sample number. iCafe is connected to MySQL database for data management and custom query. Features were arranged into five tables, recording case information, landmark coordinates, image intensity percentile for normalization (used for Nyul (31) normalization), vessel, and point features. With user-specified queries, any of the 1,456 features for each case could be retrieved for analysis. Queries can be stored in the database to be applied to any set of data with ease. Advanced queries are also achievable through SQL scripts, such as calculating the difference of length in left and right anterior proximal arteries in subjects with a complete CoW.

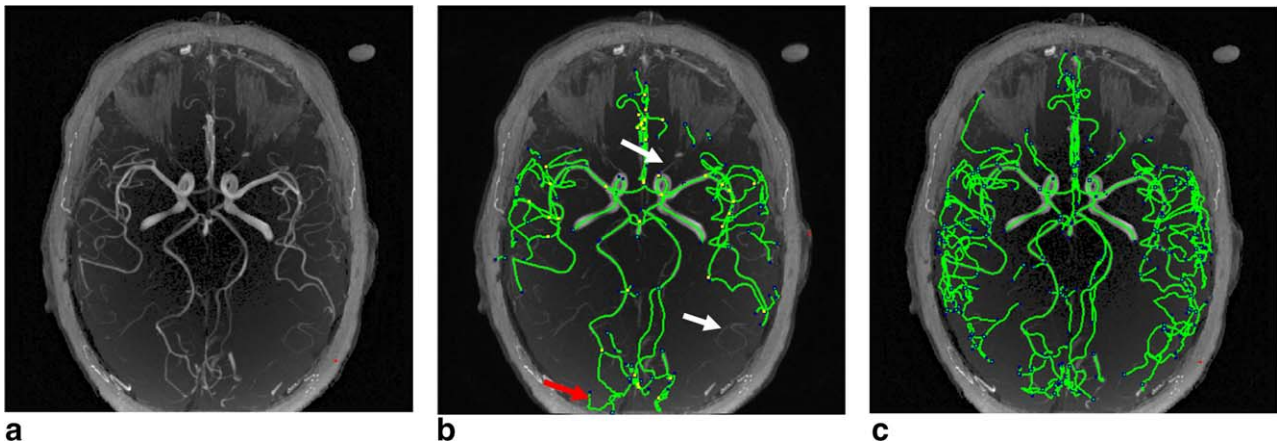

FIG. 3. (**a**) Maximum intensity projection view for a time-of-flight image. (**b**) Artery traces (green lines) using open-curve active contour model alone. Some of the false traces are marked in red arrows, and some of the missing traces are marked in white arrows. (**c**) Artery traces (green lines) using rudimentary segmentation before open-curve active contour model.

Validation

Accurate tracing results and features are important in the performance evaluation of this tool. However, validating the tracing results and features is a challenging task for human reviewers because the complicated intracranial vascular structures in 3D space make it difficult for clinicians to segment and trace all the arteries through each slice of 2D images. Therefore, we used an indirect validation method with three steps to prove the accuracy of traces and features: 1) validate the 3D position of bifurcations identified because they determine the start and end points of most traces, as well as the connections between them; 2) validate the positions of stenosis of main arteries identified because they evaluate the radius measurement of arteries; and 3) validate the length of labeled arteries (main arteries) because length is one of the most critical features from extraction and easy to measure using other methods.

Validation of the 3D Position of Bifurcations

An experienced neuroradiologist marked the 3D position of bifurcations using 2D slices of the source MRA images; neuroradiologist marked bifurcations were considered the reference standard. The bifurcation points to validate from one case were randomly chosen from all the bifurcations of the MCA, ACA, or posterior cerebral arteries (PCA). All the bifurcations from the stemming bifurcation (bifurcation of ICA/MCA/ACA for MCA or ACA branches; bifurcation of VA/PCA for PCA branches) to the most distal branches were marked by the neuroradiologist. These positions were then compared with corresponding iCafe-identified bifurcation positions. The bifurcation points that were marked by both the radiologist and detected by the algorithm were counted as agreement points, whereas those bifurcation points that were detected only by the algorithm (spurious) or only by the clinician (missed) were revisited and reviewed together by the same clinician and a separate iCafe operator to determine which were true bifurcations. In cases of nonresolution, a third rater was also consulted to adjudicate the results. Sensitivity and positive predictive values (PPV) were calculated to evaluate the performance of bifurcation points found by the algorithm. Distance between the clinician and iCafe bifurcation positions was also calculated. The radius and order (level of bifurcations starting from ICA for MCA/ACA branches; VA for PCA branches) for agreed, missed, and spurious branches were calculated to evaluate the location of agreed and disagreed bifurcations.

Validation of Stenosis Positions

Similar to the validation of bifurcation points, an experienced neuroradiologist independently marked the 3D position of stenosis using 2D slices of the original MRA images as ground truth while blinded to the iCafe analysis and patient clinical information. Due to the limitation of imaging resolution and quality, we only focused on the following large arteries or segments: $2 \times$ ICA (carotid siphon to the bifurcation of ICA/M1 (first segment of MCA)/A1 (first segment of ACA)), $2 \times$ M1, $2 \times$ A1, $2 \times$ P1 (first segment of PCA), BA (basilar artery), and $2 \times$ VA. Possible stenosis points located distal to bifurcation points were also excluded because luminal measures change between parent and daughter arteries. Then, the iCafe program generated all possible stenosis points based on the relative radius of arteries, with the calculation of the stenosis percentage based on the ratio of the radius at the maximum stenosis point over averaged radii in nearby normal artery points. We set the threshold of stenosis percentage of 10% to avoid the mild stenosis, which neuroradiologists cannot detect confidently from 2D slices or may result from noise in radius estimation. The neuroradiologist-determined points of stenosis were compared to the iCafe-generated stenosis points to determine accuracy of the program.

Validation of Artery Length Measurements

In the third step, for validation of features extracted from iCafe, length was selected for manual measurement. Vessel length was measured by manually selecting centerline points along the arteries. Experienced human

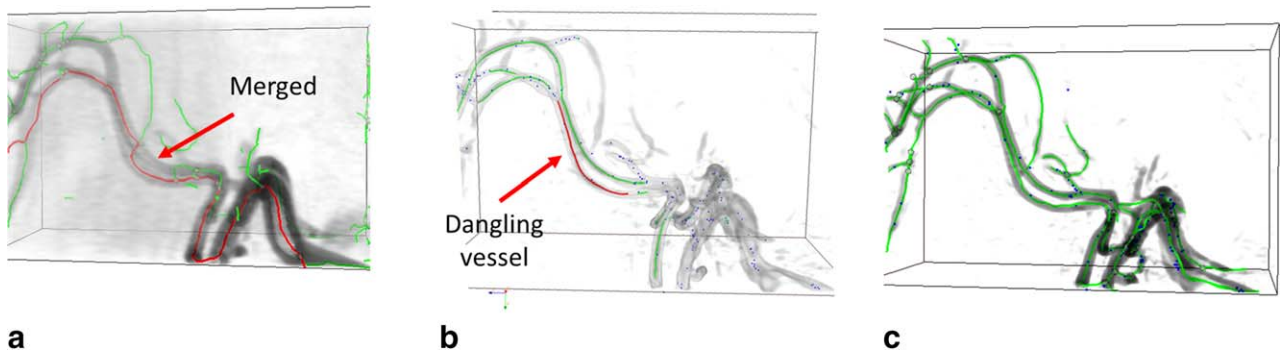

FIG. 4. (**a**) Tracing two parallel arteries directly in the raw MR angiography image by the open-curve active contour model leads to the problem of two arteries merging into one. (**b**) Tracing in the vesselness image by the open-curve active contour model leads to dangling arteries and leaves some small arteries untraced. (**c**) Tracing by combining the vesselness and raw images ensures arteries are correctly traced. Blue circles show the radius of each point.

reviewers measured M1 segments (centerlines of large arteries are easier to follow) using Philips Intellispace Portal Software v. 7.0.61310.0 (Philips Healthcare). After the centerline was drawn, length was measured on the corresponding curved planar reformat image and compared to length measurements using iCafe. The percentage of difference is calculated using Equation [1], where N is the total number of measurements, and m_{1i} and m_{2i} are the reviewer-measured and iCafe-measured length for the i th M1 segment.

$$Diff = \frac{1}{N}\sum_{i}^{N}\frac{|m_{1i}-m_{2i}|}{\frac{m_{1i}+m_{2i}}{2}} * 100\% \quad [1]$$

RESULTS

Rudimentary Segmentation

To test the importance of applying the Phansalkar local threshold method, we compared the tracing results with and without using the threshold method before tracing, as shown in Figure 3. The positions marked by arrows in Figure 3b were verified by the clinician as missing traces or incorrect traces. It should be noted that some of the isolated arteries are also traced, but if a trace is labeled with "no label" in both ends, it did not affect feature extraction results.

Improved Tracing Method

To test the effectiveness of the combined tracing method, we compared our tracing methods with tracing methods based only on the raw image and the vesselness image, as shown in Figure 4. We found the tracing method based on the raw image alone led to two parallel arteries merged into one, and the tracing method based on the vesselness image alone led to dangling vessels. The red line is the erroneously traced artery. However, the combined method can depict arteries in parallel correctly for all four cases in this experiment.

Artery Labeling

For artery labeling, the average BoI categorization accuracy by the prediction model was 98.51%. Manually changing the type of BoI allowed remaining inaccurate BoI types to be corrected. Each artery segment type was labeled with a color for better visualization in 3D view. An example is shown in Figure 5, with arteries labeled in color in MIP and 3D views.

Feature Extraction

A total of 1,456 features were extracted from each case, which were easily retrievable through the MySQL database. Examples of the key features include average radius of M1_L, distal branches length, total valid arterial volume, average normalized intensity of proximal arteries, and average CoW segments tortuosity. Results of these features from eight cases can be found in Supporting Table S3.

Processing Time

iCafe was tested on an Intel Core (Intel, Santa Clara, California, USA) i5-4210H CPU with 2.9 GHz and 16 GB RAM. The processing time for preprocessing, automatic tracing, and labeling was approximately 3 minutes. The human supervision and correction time varied by subject from 20 minutes to 1 hour.

Validation

On average, approximately 12 bifurcation points were marked by the human rater for each case. Among bifurcation points, the algorithm detected 127 points, and the human rater marked 99 points. Eighty-nine of them were agreed upon by the algorithm and human rater (having corresponding relations). The deviation distance of points was 0.328 ± 0.444 mm, which is close to the image resolution of 0.297 mm per voxel. Thirty-eight of the bifurcation points detected by the algorithm were not marked by clinician, and 10 of the bifurcation points marked by the clinician were not detected by the algorithm. Nineteen of the 38 bifurcation points only detected by the algorithm were determined to be real (i.e., were missed by the clinician in the first review). However, the remaining 19 points were spurious points detected by the algorithm. For the 10 points that the algorithm failed to detect, it was concluded in the second

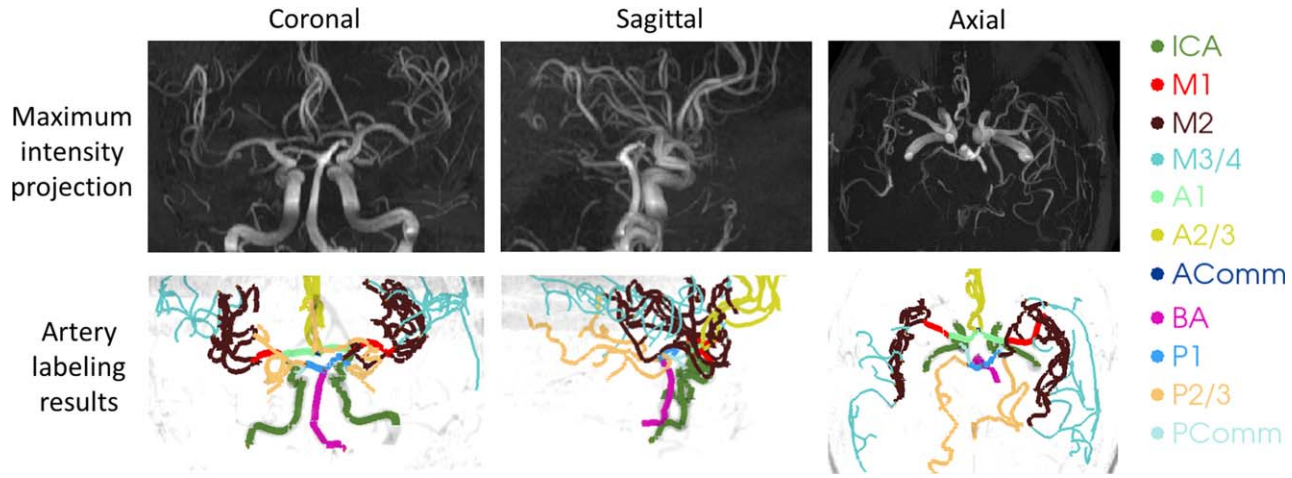

FIG. 5. Arteries labeled with their anatomical names shown with color lines in three directions of maximum intensity projection (first row) and 3D view (second row).

review that three of them were incorrect and seven were missed by algorithm. Based on this validation result, we could calculate the sensitivity of the algorithm for detecting bifurcations as $(89+19)/(89+19+7)=94\%$, the PPV as $(89+19)/(89+19+19)=85\%$, the sensitivity of the human rater as $(89+7)/(89+19+7)=83\%$, and the PPV as $(89+7)/(89+10)=97\%$.

The radius and order (level of bifurcations starting from ICA as first order for anterior circulation branches and VA as first order for posterior circulation branches, with an addition of one order for each intervening segment prior to the targeted branch point) for agreed, missed, and spurious branches are shown in Table 1. For missed bifurcations, five out of seven were tiny branches of lenticulostriate arteries near M1 branches; thus, their average radius was large and order was low. For spurious bifurcations, the smaller radius and higher order indicates they are most likely to be small branches in the distal area of the arterial tree.

The reviewer identified 13 stenosis positions among the eight cases. All the stenosis positions were deemed by the algorithm to be somewhat stenotic ($>0\%$). However, only 11 of them (sensitivity 11 of $13=85\%$) had stenosis percentage higher than the predefined threshold. Meanwhile, there were two false positive positions (PPV 11 of $13=85\%$) by the algorithm, which were considered by the reviewer as artefactual luminal narrowing due to flow dephasing resulting. We also compared average radius, vessel length, average normalized intensity, and tortuosity, which could be associated with atherosclerotic stenosis, between six stenotic artery segments and their contralateral nonstenotic counterparts (stenotic segments without contralateral counterparts were not included). The average radius on the diseased side was 0.21 mm less (P value 0.048 by paired t test), and the average normalized intensity was only 81% of the nonstenosed side (P value 0.037 by paired t test). Vessel length and tortuosity were not different between stenotic and nonstenotic side.

The reviewer-measured length of the M1 segment of the MCA was compared with the algorithm. The average difference between the two measures was 3.15%. The intraclass correlation coefficient of the two measurements was 0.97. The Bland Altman plot is shown in Figure 6.

DISCUSSION

iCafe is able to trace and label intracranial arteries and extract quantitative features from widely available TOF MRA data. Therefore, this technique provides an important method for obtaining morphometric and signal intensity features of intracranial arteries globally and regionally. iCafe measurements include information on both large and small arteries and can be a supplement to perfusion imaging (38,39). With accurate regional features from precisely labeled artery groups, iCafe presents a quantitative tool for future research, such as examining the effects of aging and disease on intracranial cerebrovasculature.

The eight MRA images were obtained from prospective scans performed in patients with intracranial atherosclerosis, providing an equivalent imaging environment to

Table 1
Number, Radius, and Order Measurement for Agreed, Missed, and Spurious Bifurcations (average ± standard deviation)

	Number	Radius of Bifurcation Branch (mm)	Order of Bifurcation Branch
Agreed bifurcations	89	0.895 ± 0.476	5.464 ± 2.884
Missed bifurcations[a]	7	1.446 ± 0.502	0.933 ± 0.294
Spurious bifurcations[b]	19	0.545 ± 0.200	5.895 ± 2.075

[a]Missed bifurcations: bifurcations identified by neuroradiologist (ground truth) but not by iCafe.
[b]Spurious bifurcations: bifurcations identified by iCafe but not by neuroradiologist (ground truth).
iCafe, intraCranial artery feature extraction.

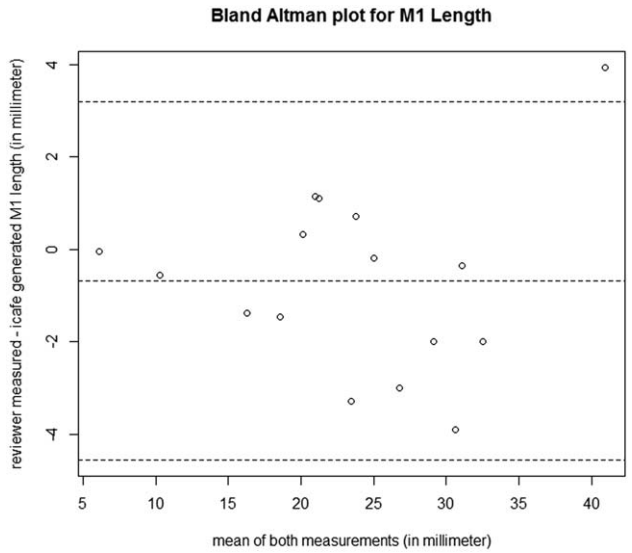

FIG. 6. Validation of length measurement of the M1 segment of the middle cerebral arteries.

vasculopathy patient populations. The performance of iCafe was evaluated on these more challenging diseased patients rather than on healthy volunteers, proving its applicability on future analysis of clinical cases.

Algorithm

Other general-purpose automatic image segmentation, or tracing tools such as 3D Slicer (24) or ImageJ (40), are likely to fail in automatic processing under complicated situations, for example, in regions with many intertwined distal MCA branches. These failures would also be difficult to identify by human supervision. iCafe is a human supervised semiautomated technique optimized for detecting and analyzing MRA. iCafe is implemented in a user-friendly graphical user interface with which operators can monitor and supervise the artery tracing and labeling process through easy operations and three different visualization methods to ensure high accuracy of extracted features.

We chose the open-curve active contour model (19) for artery tracing for the following reasons: 1) As a deformable model, the active contour model (snake) provides flexibility in tracing vessels with variable geometries; 2) the open-curve active contour model can be initialized automatically from a single seed point without a human specified contour; 3) there is precedent (13) that a neural tree reconstruction method could be adapted for MRA application; and 4) the open-curve active contour algorithm is open source under Apache License 2.0.

Because the open-curve active contour model is based on GVF with low-contrast MRA images, using the open-curve active contour model alone is inadequate to produce satisfactory results (shown in Fig. 4). Applying the Phansalkar local threshold method before tracing (in Fig. 4c) is effective in detecting smaller distal branches. The reason is that a clear background enhances gradient vectors and Frangi-filtered images, which are critical in determining the seed points and to control stretching directions of traces in the model. In addition, the segmentation also roughly confines the artery traces within the foreground region, avoiding the traces leaking to the background.

Features

A large number of features can be extracted using iCafe based on artery types and features, in contrast to previous methods. A detailed description of the artery tree and a comprehensive feature extraction may provide clinical and investigational help by identifying and characterizing pathology that may be missed with a limited number of features. In addition to common morphometric features, intensity features in each artery or vascular group are also extracted. Because the intensity value is an indicator to blood flow, intensity normalization among all the data in the database may have potential value in analyzing these intensity features.

All the information of the vascular tree is stored in a well-organized database for easy retrieval. The features are not limited to 1,456 because more customized features are available for specific tasks, such as stenosis measurement, and identification of vascular asymmetries between the left and right hemispheres.

Validation

Precise characterization of vascular anatomy is important for understanding cerebrovascular diseases (41).

Detailed human tracing of the intracranial arterial tree is difficult, which was the impetus for the development of iCafe. The challenges of tracing intracranial arteries lie in the precise identification of branching points. To validate a comprehensive intracranial artery map, previously used methods such as observing the tracings in a perpendicular view (13) are insufficient. In our study, bifurcation and stenosis points along arterial branches were marked and compared, which is more robust and allows tracing accuracy validation. Additionally, length measurements were compared with results from a commercially used measurement software. These validation experiments provide preliminary support that iCafe-extracted features can be used in future analysis in large population-based studies.

The deviation between the expert-marked and iCafe-traced bifurcation points approximated the imaging resolution, indicating minimal difference. The high sensitivity and PPV indicate that bifurcation positions detected by iCafe are valid and accurate. We also found that most disagreements in the position of bifurcations were small branching arteries with relatively low signal.

It should be noted that the identification of bifurcation points is a challenging task, even for expert human reviewers. Missing and deviated bifurcation points arise for many reasons, such as low signal near branch ends caused by slow or in-plane flow, very small arteries located close to large arteries, and irregular branching patterns.

The validation of stenosis positions is aimed at proving the accuracy of radius measurements of traces and exploring its potential clinical uses. The high sensitivity and PPV of stenosis detection has shown that iCafe can

accurately describe radius variations along artery segments. With further validation, iCafe could serve as an initial clinical evaluation tool to lessen the burden on radiologists in MRA.

Feature differences between diseased artery segments and the normal contralateral side indicate that iCafe could potentially contribute biomarkers for vascular disease analysis in future research. More investigation is necessary, however.

Due to the limitation of human measurement, only length of large arteries was assessed for feature validation. The difference between human-measured and iCafe-generated M1 segment length was low. Any difference in results may have occurred from the reconstruction when converting 3D images to 2D for manual measurement. In addition, the number of centerline points that a human reviewer selected will also influence the measurement. Overall, the validation showed a high level of agreement.

Limitations

Although a large number of features can be derived using iCafe, only a limited set (bifurcation, stenosis positions, and vessel length) were validated in the current study. This limitation is mainly due to the difficulty in obtaining human-based tracing of the entire vasculature and the limitations of currently available measurement tools.

iCafe was implemented using C++ on the Windows platform (Microsoft Corporation, Redmond, Washington, USA) only. Because the underlying graphical user interface framework is cross-platform-supported, iCafe can be further developed on other platforms to meet the needs of different clinical and research environments.

Three-dimensional TOF MRA images were used to test iCafe, but we believe with some modifications that iCafe could be applied to other bright blood-imaging techniques such as contrast-enhanced MRA, CT angiography, or 3D digital subtraction angiography.

The processing time is between 20 minutes to 1 hour, mostly due to time needed for human intervention and correction during the manual editing stage. A fully automated algorithm will help to reduce processing time, allowing for better clinical access. More powerful and accurate automated tracing and labeling methods are planned for future development.

CONCLUSION

A semiautomated quantitative measurement tool for intracranial arteries from 3D TOF MRA images has been developed and shown to provide accurate tracing of intracranial arteries. Through its ability to provide novel imaging biomarkers for cerebrovascular disease, it may facilitate new research and clinical approaches.

ACKNOWLEDGMENTS

The following members of the Vascular Imaging Laboratory at the University of Washington provided assistance for this project: Hiroko Watase, Baocheng (Paul) Chu, Haifeng Gao for anatomical knowledge used to design this tool, and Daniel S. Hippe for statistical consultation. We also thank Yu Wang from the Rensselaer Polytechnic Institute for providing the open-source code for open-curve snake tracing.

REFERENCES

1. Roher AE, Tyas SL, Maarouf CL, et al. Intracranial atherosclerosis as a contributing factor to Alzheimer's disease dementia. Alzheimer's Dement 2011;7:436–444.
2. Arvanitakis Z, Capuano AW, Leurgans SE, Bennett DA, Schneider JA. Relation of cerebral vessel disease to Alzheimer's disease dementia and cognitive function in elderly people: a cross-sectional study. Lancet Neurol 2016;15:934–943.
3. Hinshaw WS, Bottomley PA, Holland GN. Radiographic thin-section image of the human wrist by nuclear magnetic resonance. Nature 1977;270:722–723.
4. Wright VL, Olan W, Dick B, Yu H, Alberts-Grill N, Latour LL, Baird AE. Assessment of CE-MRA for the rapid detection of supra-aortic vascular disease. Neurology 2005;65:27–32.
5. Scarabino T, Carriero A, Giannatempo GM, Marano R, De Matthaeis P, Bonomo L, Salvolini U. Contrast-enhanced MR angiography (CE MRA) in the study of the carotid stenosis: comparison with digital subtraction angiography (DSA). J Neuroradiol 1999;26:87–91.
6. Röther J, Schwartz A, Wentz KU, Rautenberg W, Hennerici M. Middle cerebral artery stenoses: assessment by magnetic resonance angiography and transcranial doppler ultrasound. Cerebrovasc Dis 1994;4:273–279.
7. Alpers BJ, Berry RG, Paddison RM. Anatomical studies of the circle of Willis in normal brain. Arch Neurol Psychiatry 1959;81:409.
8. Yan P, Kassim AA. Segmentation of volumetric MRA images by using capillary active contour. Med Image Anal 2006;10:317–329.
9. Wang R, Li C, Wang J, Wei X, Li Y, Zhu Y, Zhang S. Threshold segmentation algorithm for automatic extraction of cerebral vessels from brain magnetic resonance angiography images. J Neurosci Methods 2015;241:30–36.
10. Adame IM, de Koning PJH, Lelieveldt BPF, Wasserman BA, Reiber JHC, van der Geest RJ. An integrated automated analysis method for quantifying vessel stenosis and plaque burden from carotid MRI images. Stroke 2006;37:2162–2164.
11. Bullitt E, Rahman FN, Smith JK, Kim E, Zeng D, Katz LM, Marks BL. The effect of exercise on the cerebral vasculature of healthy aged subjects as visualized by MR angiography. Am J Neuroradiol 2009;30:1857–1863.
12. Bullitt E, Zeng D, Mortamet B, Ghosh A, Aylward SR, Lin W, Marks BL, Smith K. The effects of healthy aging on intracerebral blood vessels visualized by magnetic resonance angiography. Neurobiol Aging 2010;31:290–300.
13. Wright SN, Kochunov P, Mut F, Bergamino M, Brown KM, Mazziotta JC, Toga AW, Cebral JR, Ascoli GA. Digital reconstruction and morphometric analysis of human brain arterial vasculature from magnetic resonance angiography. Neuroimage 2013;82:170–181.
14. Krishnan MMR, Faust O. Automated glaucoma detection using hybrid feature extraction in retinal fundus images. J Mech Med Biol 2013;13:1350011.
15. Can A, Shen H, Turner JN, Tanenbaum HL, Roysam B. Rapid automated tracing and feature extraction from retinal fundus images using direct exploratory algorithms. IEEE Trans Inf Technol Biomed 1999;3:125–138.
16. Metz CT, Schaap M, Weustink AC, Mollet NR, van Walsum T, Niessen WJ. Coronary centerline extraction from CT coronary angiography images using a minimum cost path approach. Med Phys 2009;36:5568.
17. Yang G, Kitslaar P, Frenay M, Broersen A, Boogers MJ, Bax JJ, Reiber JHC, Dijkstra J. Automatic centerline extraction of coronary arteries in coronary computed tomographic angiography. Int J Cardiovasc Imaging 2012;28:921–933.
18. Kass M, Witkin A, Terzopoulos D. Snakes: active contour models. Int J Comput Vis 1988;1:321–331.
19. Wang Y, Narayanaswamy A, Tsai CL, Roysam B. A broadly applicable 3-D neuron tracing method based on open-curve snake. Neuroinformatics 2011;9:193–217.

20. Choromanska A, Chang S-F, Yuste R. Automatic reconstruction of neural morphologies with multi-scale tracking. Front Neural Circuits 2012;6:25.
21. Peng H, Hawrylycz M, Roskams J, Hill S, Spruston N, Meijering E, Ascoli GA. BigNeuron: large-scale 3D neuron reconstruction from optical microscopy images. Neuron 2015;87:252–256.
22. Wang Y, Narayanaswamy A, Roysam B. Novel 4-D open-curve active contour and curve completion approach for automated tree structure extraction. Proc IEEE Comput Soc Conf Comput Vis Pattern Recognit 2011:1105–1112.
23. Zhang D, Wang C, Zhou S. A new method of vessel centerline extraction from 3D CT coronary angiography based on open-snake. (ICBISP 2015). 2015 IET International Conference on Biomedical Image and Signal Processing, Beijing, China, 2015. p. 1–5. doi: 10.1049/cp.2015.0771.
24. Fedorov A, Beichel R, Kalpathy-Cramer J, et al. 3D Slicer as an image computing platform for the Quantitative Imaging Network. Magn Reson Imaging 2012;30:1323–1341.
25. Peng H, Ruan Z, Long F, Simpson JH, Myers EW. V3D enables real-time 3D visualization and quantitative analysis of large-scale biological image data sets. Nat Biotechnol 2010;28:348–353.
26. Bash S, Villablanca JP, Jahan R, Duckwiler G, Tillis M, Kidwell C, Saver J, Sayre J. Intracranial vascular stenosis and occlusive disease: Evaluation with CT angiography, MR angiography, and digital subtraction angiography. Am J Neuroradiol 2005;26:1012–1021.
27. Boussel L, Rayz V, McCulloch C, Martin A, Acevedo-Bolton G, Lawton M, Higashida R, Smith WS, Young WL, Saloner D. Aneurysm growth occurs at region of low wall shear stress: patient-specific correlation of hemodynamics and growth in a longitudinal study. Stroke 2008;39:2997–3002.
28. Cheung AT, Harmatz P, Wun T, Chen PC, Larkin EC, Adams RJ, Vichinsky EP. Correlation of abnormal intracranial vessel velocity, measured by transcranial Doppler ultrasonography, with abnormal conjunctival vessel velocity, measured by computer-assisted intravital microscopy, in sickle cell disease. Blood 2001;97:3401–3404.
29. Tschirren J, McLennan G, Palágyi K, Hoffman EA, Sonka M. Matching and anatomical labeling of human airway tree. IEEE Trans Med Imaging 2005;24:1540–1547.
30. Bogunović H, Pozo JM, Cardenes R, Roman LS, Frangi AF. Anatomical labeling of the circle of willis using maximum a posteriori probability estimation. IEEE Trans Med Imaging 2013;32:1587–1599.
31. Nyul LG, Udupa JK, Zhang X. New variants of a method of MRI scale standardization. IEEE Trans Med Imaging 2000;19:143–150.
32. Phansalkar N, More S, Sabale A, Joshi M. Adaptive local thresholding for detection of nuclei in diversity stained cytology images. (ICCSP 2011). 2011 International Conference on Communications and Signal Processing, Calicut, Kerala, India, 2011. p. 218–220. doi: 10.1109/ICCSP.2011.5739305.
33. Kapur JN, Sahoo PK, Wong AKC. A new method for gray-level picture thresholding using the entropy of the histogram. Comput Vision Graph Image Process 1985;29:273–285.
34. Frangi AF, Niessen WJ, Vincken KL, Viergever MA. Multiscale vessel enhancement filtering. In Medial Image Computing and Computer-Assisted Intervention. MICCAI'98. Lecture Notes in Computer Science 1998;1496:1496:130–137. doi: 10.1016/j.media.2004.08.001.
35. Hsu C-Y, Ghaffari M, Alaraj A, Flannery M, Zhou XJ, Linninger A. Gap-free segmentation of vascular networks with automatic image processing pipeline. Comput Biol Med 2017;82:29–39.
36. Chen L, Wang D. An improved acquaintance immunization strategy for complex network. J Theor Biol 2015;385:58–65.
37. Cannon R, Turner D, Pyapali G, Wheal H. An on-line archive of reconstructed hippocampal neurons. J Neurosci Methods 1998;84:49–54.
38. Petrella JR, Provenzale JM. MR perfusion imaging of the brain: techniques and applications. AJR Am J Roentgenol 2000;175:207–219.
39. Korfiatis P, Erickson B. The basics of diffusion and perfusion imaging in brain tumors. Appl Radiol 2014;43:22–29.
40. Schindelin J, Rueden CT, Hiner MC, Eliceiri KW. The ImageJ ecosystem: an open platform for biomedical image analysis. Mol Reprod Dev 2015;82:518–529.
41. O'Flynn PM, O'Sullivan G, Pandit AS. Methods for three-dimensional geometric characterization of the arterial vasculature. Ann Biomed Eng 2007;35:1368–1381.

SUPPORTING INFORMATION

Additional supporting information may be found in the online version of this article.

Table S1. Intracranial artery segments classified in iCafe
Table S2. Definition of vascular groups
Table S3. Example features extracted from iCafe (Average ± standard deviation of eight cases processed)